Stem Cell Reports

Report

Therapeutic Regeneration of Lymphatic and Immune Cell Functions upon Lympho-organoid Transplantation

Elisa Lenti,[1] Silvia Bianchessi,[1] Steven T. Proulx,[2] Maria Teresa Palano,[1] Luca Genovese,[1] Laura Raccosta,[3] Antonello Spinelli,[4] Denise Drago,[5] Annapaola Andolfo,[5] Massimo Alfano,[6] Tatiana V. Petrova,[7] Sylvain Mukenge,[8] Vincenzo Russo,[3] and Andrea Brendolan[1,*]

[1]Unit of Lymphoid Organ Development, Division of Experimental Oncology, DIBIT-1 3A2, IRCCS San Raffaele Scientific Institute, Via Olgettina 60, 20132 Milan, Italy
[2]Institute of Pharmaceutical Sciences, Swiss Federal Institute of Technology, ETH Zurich, 8093 Zurich, Switzerland
[3]Unit of Immuno-Biotherapy of Melanoma and Solid Tumors, Division of Experimental Oncology, IRCCS San Raffaele Scientific Institute, 20132 Milan, Italy
[4]Experimental Imaging Centre, IRCCS San Raffaele Scientific Institute, 20132 Milan, Italy
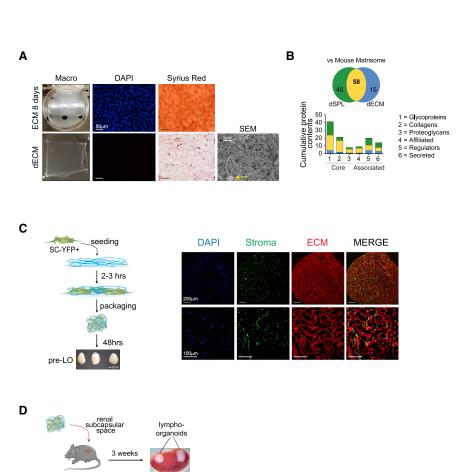[5]ProMiFa, Protein Microsequencing Facility, IRCCS San Raffaele Scientific Institute, 20132 Milan, Italy
[6]Division of Experimental Oncology/Unit of Urology, URI, IRCCS Ospedale San Raffaele, Milan, Italy
[7]Department of Oncology, University of Lausanne, and Ludwig Institute for Cancer Research, 1066 Lausanne, Switzerland
[8]Department of Hepatobiliary Surgery, IRCCS San Raffaele Hospital, 20132 Milan, Italy
*Correspondence: brendolan.andrea@hsr.it
https://doi.org/10.1016/j.stemcr.2019.04.021

SUMMARY

Lymph nodes (LNs) are secondary lymphoid tissues that play a critical role in filtering the lymph and promoting adaptive immune responses. Surgical resection of LNs, radiation therapy, or infections may damage lymphatic vasculature and compromise immune functions. Here, we describe the generation of functional synthetic lympho-organoids (LOs) using LN stromal progenitors and decellularized extracellular matrix-based scaffolds, two basic constituents of secondary lymphoid tissues. We show that upon transplantation at the site of resected LNs, LOs become integrated into the endogenous lymphatic vasculature and efficiently restore lymphatic drainage and perfusion. Upon immunization, LOs support the activation of antigen-specific immune responses, thus acquiring properties of native lymphoid tissues. These findings provide a proof-of-concept strategy for the development of functional lympho-organoids suitable for restoring lymphatic and immune cell functions.

INTRODUCTION

Lymph node (LN) development is a multistep process involving crosstalk of multiple cell types and culminating in integration of LNs into the lymphatic system (Brendolan and Caamano, 2012; Onder and Ludewig, 2018). Non-hematopoietic stromal progenitors of lymphoid organs play critical roles in tissue development, organization, and function through the secretion of cytokines, chemokines, and the extracellular matrix (ECM), a tri-dimensional scaffold that provides structural support and anchorage for cells (Benezech et al., 2012; Lokmic et al., 2008; Onder et al., 2017; Petrova and Koh, 2018). Afferent-collecting lymphatics transport lymph and antigens to the LN where immune responses are generated (Petrova and Koh, 2018). However, surgical resection of LNs, radiation therapy, or infections may damage the lymphatic vasculature and contribute to secondary lymphedema, a chronic disease characterized by excessive tissue swelling, fibrosis, and decreased immune responses (Alitalo, 2011). Currently available lymphedema treatments are limited to manual lymph drainage and compression garments, and definitive therapeutic options are still lacking (Andersen et al., 2000). Vascularized autologous lymph node transfer (ALNT), a surgical procedure in which a LN flap is harvested and transplanted at the site of resected LNs to improve lymphatic

drainage, is emerging as a therapeutic option for the treatment of cancer-associated lymphedema (Becker et al., 2006; Kanapathy et al., 2014; Scaglioni et al., 2018). Although feasible, such an approach requires surgical intervention and can be associated with donor-site complications, which may limit its application (Gould et al., 2018).

To circumvent these problems, tissue engineering may provide strategies to develop artificial lymphoid tissues for applications in regenerative medicine (Nosenko et al., 2016; Purwada et al., 2015; Cupedo et al., 2012). It has been demonstrated that transplantation under the kidney capsule of an engineered stromal cell line expressing lymphotoxin α in a biocompatible scaffold or the delivery of stromal-derived chemokines in hydrogel is sufficient to promote the organization of lymphoid-like structures with immunological function (Castagnaro et al., 2013; Suematsu and Watanabe, 2004; Kobayashi and Watanabe, 2016). Whether these approaches contribute to regenerate immune and lymphatic functions in preclinical models of LN resection remains unknown.

Here, we generated lympho-organoids (LOs) using LN stromal progenitors in an ECM-based scaffold and show that LO transplantation at the site of resected LN contributes to restoration of lymphatic and immune functions. Upon transplantation, LOs are integrated into the endogenous lymphatic vasculature and efficiently restore lymphatic

Figure 1. Generation of Vascularized Lympho-Organoids Using Lymphoid Stromal Progenitors and ECM-Based Scaffold

(A) Macroscopic view of ECM before and after decellularization, DAPI (nuclei), and Sirius red (collagens) staining. Representative scanning electron microscopy (SEM) image to visualize the dense network of collagen fibers and the presence of glycosaminoglycan aggregates (yellow arrow). Scale bars: 50 μm (DAPI and Sirius red) and 1 μm (SEM).

(B) Nano-liquid chromatography mass spectrometry analysis. Graph indicate commonalities in protein identities.

(C) Scheme of YFP+ stromal progenitors cultured on top of the dECM in a tri-dimensional (3D) configuration for 48 h, and macroscopic view of the resulting pre-assembled LOs (pre-LOs). Representative confocal images of tissue sections stained for YFP (Stroma, in green) and for COLL-IV (ECM, in red). Nuclei visualized by DAPI. Scale bars: 200 μm and 100 μm.

(D) Scheme of transplantation of pre-LOs to the mouse renal subcapsular space of *Prox1*-mOrange2 reporter mice. Graph represents the number of mice containing clusters of lymphoid cells (15 mice analyzed in total). Representative confocal images of LOs 3 weeks after transplant. Tissue sections were stained for CD3 (T cell; red, upper panel), B220 (B cells; gray, upper panel), PECAM-1 (blood endothelial cells; red, lower panel), PROX-1 (lymphatic endothelial cells; green, lower panel), and DAPI (nuclei; blue) to visualize nuclei and identify B/T cell clusters. Scale bars: 100 μm and 50 μm. Images are representative of three independent experiments.

drainage and perfusion. Notably, upon immunization, LOs support the activation of antigen-specific immune responses and acquire properties of native lymphoid tissues. These findings provide a robust preclinical approach for the development of synthetic LOs capable of regenerating lymphatic and immune functions.

RESULTS AND DISCUSSION

Generation of Vascularized Lympho-Organoids Using a Decellularized Stromal ECM-Based Scaffold and Lymphoid Stromal Progenitors

We hypothesized that the delivery of primary LNs stromal progenitors embedded in a physiological ECM-based scaffold may be sufficient to initiate the organization of functional LOs. To this end, we first generated an ECM-based scaffold by culturing a spleen stromal cell line in the presence of ascorbate, that promotes collagen deposition (Figure S1A) (Franco-Barraza et al., 2016; Genovese et al., 2014). At day 10 of treatment, stromal cells formed a densely packed monolayer that was decellularized using a previously published protocol adapted to our culture conditions (Figures S1A and 1A) (Franco-Barraza et al., 2016; Genovese et al., 2014). The decellularized ECM (dECM) appeared as a thin and elastic layer characterized by a network of collagen fibers that was confirmed by ultrastructural analysis using scanning electron microscopy (Figure 1A). Lectin-peanut agglutinin (PNA) staining also revealed the presence of ECM-associated glycoproteins (Figure S1B).

To gain insights into the proteomic landscape, we performed mass spectrometry (MS) analysis and related the composition of the dECM to that of a decellularized splenic tissue (dSPL) (Figure 1B). The list of proteins obtained (ProteomeXchange: PXD013250) was compared with that of proteins annotated in the Mouse Matrisome Database atlas, a database of all known ECM proteins (Naba et al., 2016). The results showed a large degree of similarities between the two tissues with 58 (60%) common proteins out of 113 not significantly different in dSPL versus dECM (p < 0.01) (Figure 1B and Table S1). Notably, the dECM contained components of the interstitial matrix (Collagens I and III, FN, TN-C), basement membrane (COLL-IV, LAM-α5, NID2), and secreted proteins and regulators of ECM biology, indicating that its composition is more physiological compared with commercially available scaffolds, which are mostly made of single ECM components.

To assess the ability of dECM to promote stromal cell adhesion, we isolated primary LN stromal progenitors from neonatal mice and expanded them for 10 days *in vitro*. The phenotypic analysis revealed the presence of a homogeneous population of non-endothelial GP38^{+} stromal progenitors (Figure S2A). These stromal progenitors, when seeded on top of the dECM, firmly adhered to the matrix and showed an elongated arrangement (Figure S1C). We then pre-assembled a lympho-organoid (pre-LO) by culturing stromal progenitors isolated from green fluorescence reporter mice onto the dECM in a three-dimensional (3D) configuration for 48 h (Figure 1C). The resulting structures appeared compacted and resembled native LNs in shape and dimensions (Figure 1C). Immunofluorescence staining revealed a network of stromal precursors adherent to the dECM and evenly distributed throughout the organoid (Figure 1C). To assess whether pre-LOs support vascularization and infiltration of lymphoid cells, we transplanted them under the mouse renal subcapsular space (Figure 1D). Three weeks later, the grafts appeared larger compared with that originally transplanted, and immunofluorescence staining revealed that a large fraction (50%) of LOs contained clusters of CD3^{+} T and B220^{+} B cells together with blood (PECAM-1^{+}) and lymphatic (PROX-1^{+}) endothelial cells (Figure 1D). Altogether, these findings indicate that the transplantation of pre-LOs generated with basic constituents of lymphoid organs is sufficient to initiate organization of LOs with features of native tissues.

Transplantation of Lympho-Organoids at the Site of Resected Lymph Nodes Restores Lymphatic Drainage

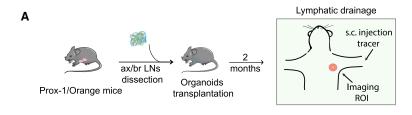To assess whether LOs are functional in restoring lymphatic drainage, we exploited an approach in which the surgical dissection of axillary/brachial LNs models the resection of LNs during cancer surgery, a procedure that contributes to the development of lymphedema (Blum et al., 2013). Although in mice this procedure does not cause macroscopic lymphedema, because of their small size and minimal lymphatic pressure gradients, it allows us to evaluate whether transplanted LOs contribute to lymphatic drainage. To this end, we performed resection of axillary/brachial LNs together with a small portion of the surrounding fat pad and lymphatics, which was followed by LO transplantation (Figure 2A). Two months later, lymphatic drainage was evaluated by measuring near-infrared (NIR) fluorescence imaging in the region of the axilla receiving the LO transfer (Proulx et al., 2013, 2017). Two minutes after injecting the P20D800 tracer in the dorsal skin of the paw, we quantified by NIR imaging the intensity of the region of interest (ROI) signal over the axilla region. This analysis revealed that the signal from the ROI of mice receiving pre-LOs (dECM + stromal progenitors) after LN resection was comparable with that of sham-operated control mice; whereas axillary LN-resected mice with or without the dECM (alone) showed low or no signal (Figure 2B). Notably, microcomputed tomography (μCT imaging) confirmed the presence of a well-defined 3D structure in the axillary region only in pre-LO transplanted and sham-operated control mice (Figure 2B).
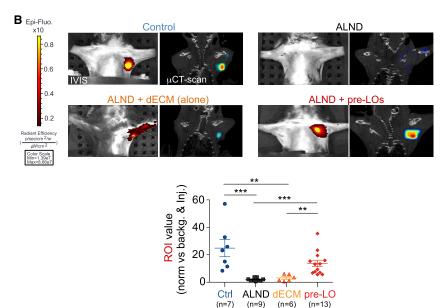
Lympho-Organoids Are Integrated into Pre-existing Lymphatics and Support Lymphatic Perfusion

We then assessed whether transplanted LOs are perfused and connected to endogenous LNs, a requisite for proper lymphatic function. To test this, we measured lymphatic perfusion after popliteal LN resection followed by LO transplantation. To visualize endogenous lymphatics, we used reporter mice, which express an mOrange fluorescence signal under the *Prox-1* promoter (Figure 3A). One month later, imaging of mice injected intradermally with fluorescein isothiocyanate (FITC)-dextran revealed a dense network of FITC[+]PROX1^{+} endogenous lymphatic vessels surrounding and connecting to LOs (Figure 3B).

Longitudinal FITC and NIR imaging of the lymphatic vasculature in transplanted limbs showed perfusion of both the popliteal efferent vessel (EV) and the downstream sacral LN (saLN) (Figures 3B and S3), suggesting that LOs were integrated into the existing lymphatics and acquired the capacity to support lymphatic perfusion. Notably, quantification analysis revealed saLN perfusion in a significantly higher fraction (67%) of mice receiving LO transfer compared with those that did not receive LOs (11%), whereas no differences were observed in terms of dermal backflow or afferent vessel perfusion between the two groups (Figure 3D, Videos S1 and S2).

A

Prox-1/Orange mice → ax/br LNs dissection → Organoids transplantation → 2 months → Lymphatic drainage — s.c. injection tracer, Imaging ROI

B

Epi-Fluo. x10

Control · ALND

IVIS · µCT-scan

ALND + dECM (alone) · ALND + pre-LOs

Radiant Efficiency $\frac{p/sec/cm^2/sr}{\mu W/cm^2}$

Color Scale Min=1.39e7 Max=8.66e7

ROI value (norm vs backg. & Inj.)

Ctrl (n=7) · ALND (n=9) · dECM (n=6) · pre-LO (n=13)

Figure 2. Transplantation of Lympho-Organoids at the Site of LN Resection Promotes Lymphatic Drainage

(A) Scheme of transplantation of pre-LOs in place of axillary/brachial dissected LNs.

(B) Representative images of the intensity signal at the region of interest (ROI) through live imaging (IVIS) and µCT-Scan showing the localization of LOs. Mouse groups: control, sham-operated; ALND, axillary LN dissected; ALND + dECM (alone), axillary LN dissected and transplanted with dECM alone; ALND + pre-LO, axillary LN dissected and transplanted with dECM and primary stromal progenitors. Quantification analysis of the ROI value (normalized versus background and signal at site of injection) for each mouse analyzed. Data presented as means ± SD from three independent experiments; n, total number of mice analyzed for each experimental group. Statistically significant comparisons: **$p < 0.01$ and ***$p < 0.001$.

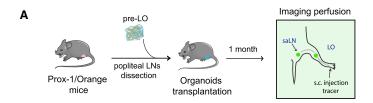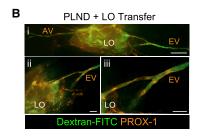## Lympho-Organoids Contain T and B Cell Clusters and Support Antigen-Specific Immunity

Based on these findings, we tested whether LOs transplanted at the site of LN dissection become functional as a reservoir of immune cells, a feature characteristic of lymphoid tissues. Immunofluorescence staining performed on LOs transplanted at the site of popliteal LN showed the presence of PECAM-1^{+} blood and LYVE-1^{+} lymphatic endothelial cells (Figure 4A). Notably, around 70% of the harvested LOs (20 of 29) appeared highly infiltrated with lymphoid cells. Among these, 60% of LOs contained clearly segregated clusters of T and B cells (Figure 4B), often associated with networks of CD35^{+} follicular dendritic cells (Figure 4B), whereas the remaining 40% contained many infiltrated T cells with only a few B cells (data not shown).
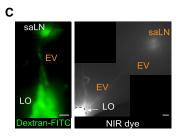
A requisite of LN functionality is the ability to mount antigen-specific immune responses (Lim et al., 2016). To test whether LOs have acquired this capability, we performed LO transplantation at the popliteal site followed by injection of CD8^{+} OT-I cells (5×10^6/mouse) (Russo et al., 2007). Twenty-four hours later, mice were

immunized intradermally in the footpad of the transplanted limb with ovalbumin (OVA)-peptide SIINFEKL in adjuvant (OT-I + OVA) or received saline as a control (OT-I) (Figure 4C). LOs and inguinal LNs (iLNs) were collected 5 days post immunization, and the frequency of OT-I CD8^{+} T cells was measured by fluorescence-activated cell sorter (FACS) staining of the Vα2 and Vβ5.1 chains of the transgenic (OT-I) T cell receptor. Notably, LOs of immunized mice contained a substantial higher percentage OT-I CD8^{+} T cells compared with control mice, while the frequency of OT-I cells in iLNs was similar between the two groups (Figure 4C). These findings indicate that transplanted LOs acquire immunological function.

To our knowledge, this is the first study to demonstrate the feasibility of *ex vivo* pre-assembled synthetic LOs for the therapeutic restoration of lymphatic and immune cell functions in preclinical models. We have provided a clinically relevant proof-of-concept approach to show that two basic constituents of developing LN, lymphoid stromal progenitors and the ECM, are sufficient to promote *in vivo* self-organization of functional LOs for tissue
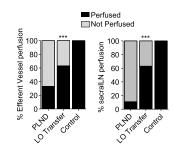
Figure 3. Lympho-Organoids Are Connected to Lymphatics and Promote Lymphatic Perfusion

(A) Scheme of pre-LO transplantation at the site of popliteal dissected LNs.

(B) Representative fluorescence images of LO surrounded and infiltrated by FITC⁺PROX-1⁺ lymphatics (orange). Insets ii and iii are magnifications from panel i. AV, afferent vessel; EV, efferent vessel, LO, lympho-organoid. Scale bars: 500 μm (panel i) and 200 μm (ii and iii). Images are representative of two independent experiments.

(C) Representative FITC and NIR fluorescence images of lymphatic vasculature showing connections between LOs and saLN through EV. EV, efferent vessel; LO, lympho-organoid; saLN, sacral LN. Images are representative of two independent experiments. Scale bars: 1,000 μm.

(D) Quantification analysis of lymphatic perfusion. Data presented as pooled number of mice used from two independent experiments. ***p < 0.001.

	Popl. EV perfusion	saLN perfusion	Dermal Backflow	AV to popl. region
PLND (popLN dissected)	3/9 (33%)	1/9 (11%)	7/9 (77%)	9/9 (100%)
PLND + LO transfer	12/18 (67%)	12/18 (67%)	11/18 (61%)	18/18 (100%)
Control (Sham-Operated)	3/3 (100%)	3/3 (100%)	1/3 (33%)	3/3 (100%)

regeneration. Stromal cells may facilitate adhesion and retention of lymphoid cells into the dECM and promote integration of LO into lymphatics via secretion of lymphangiogenic factors contributing to LO function. Our findings indicate that after transplantation, LOs remains for at least 2 months, although it remains unclear if they endure over a longer period. Nevertheless, our findings indicate that LOs may represent a therapeutic approach to restore lymphatic and immune cell functions in secondary lymphedema and other diseases in which LNs have been removed or are dysfunctional.

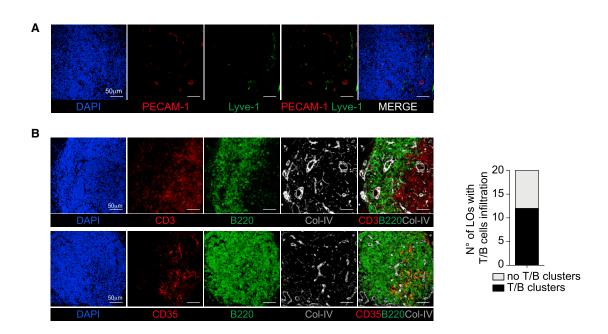## EXPERIMENTAL PROCEDURES

Mice

Prox1-mOrange2 mice have been described previously (Hagerling et al., 2011). C57BL/6N mice were purchased from Charles River, Italy. Animals were maintained in a specific pathogen-free animal facility and treated in accordance with European Union and Institutional Animal Care and Use Committee guidelines.

Cell Cultures and ECM Production

The immortalized stromal cell (iSC) line used for dECM preparation has been previously described (Farinello et al., 2018). Cells were cultured in Dulbecco's modified Eagle's medium (DMEM; Gibco) supplemented with 10% fetal bovine serum (FBS; Euroclone), 1% L-glutamine (Gibco-Invitrogen), and 1% penicillin (Gibco-Invitrogen) and incubated at 37°C with 5% CO₂. Cells were split every 2 days using Trypsin (Gibco-Invitrogen), and washing steps were performed with PBS 1×. Primary stromal progenitors (pSP) were obtained from neonatal mesenteric lymph nodes (mLNs). mLNs were digested with 0.45 mg/mL Liberase TM (05401119001, Roche) in a 1:1 ratio with FBS for 20 min at 37°C under gentle shaking and pipetting every 10 min. mLN primary cell suspensions were seeded into 10 cm dishes and cultured for 4 days. Primary cells were trypsinized, expanded, and cultured for a maximum of 7–10 days, then used for LO generation. Each primary cell preparation was tested using FACS to assess the phenotype (detailed FACS analysis in Figure S2). For generation of dECM, 8 × 10⁵ cells were seeded on 0.2% gelatin-coated 60 mm Petri dishes and cultured to reach 80% confluence the day after. Then, the medium was changed and supplemented with 50 μg/mL of ascorbic acid (A4544, Sigma). The medium was changed every second day (day 2, 4, 6, 8), and at day 10, the cell layer was decellularized using a protocol previously published and adapted to our culture conditions (Genovese et al., 2014). All the decellularization steps were performed on a rotating shaker, and the resulting dECM was washed with PBS 1× and stored under PBS 1× supplemented with 1% penicillin/streptomycin at 4°C for up to 1 month.
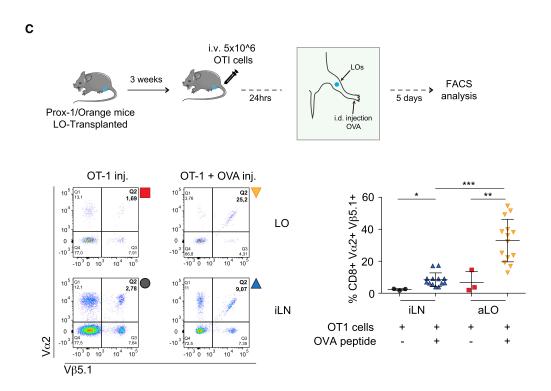
Figure 4. Lympho-Organoids Support the Generation of Antigen-Specific Immunity

(A) Representative confocal images of transplanted LOs stained for DAPI (nuclei; blue), PECAM-1 (blood endothelial cells; red), and LYVE-1 (lymphatic endothelial cells; green). Scale bars: 50 μm. Images are representative of LOs from three independent experiments.

(B) Representative confocal images of LOs stained for DAPI (nuclei, blue), CD3 (T cells; red, upper panel), CD35 (follicular dendritic cells; red, lower panel), B220 (B cells; green), and Collagen-IV (ECM; white). Graph represents the number of mice containing clusters of lymphoid cells. Images are representative of LOs from three independent experiments.

(legend continued on next page)

ECM Purification and Protein Identification Using Nano-Liquid Chromatography MS/MS Analysis

Spleens were collected from three different C57BL6/N mice, and spleen-derived ECM (dSPL) was prepared as described previously (Genovese et al., 2014). The dECM sample was a pool of ten dECMs from three different decellularizations. ECM proteins were extracted, quantified, and processed by nano-liquid chromatography MS/MS analysis. For quantification of proteins, the raw data were loaded into MaxQuant software version 1.5.2.8; label-free protein quantification was determined on the intensities of precursors, both as protein intensities and normalized protein intensities (LFQ intensities). Peptides and proteins were accepted with a false discovery rate less than 1% and a minimum of two peptides per protein with one unique. The proteins identified by proteomic analysis were compared with the Total Mouse Matrisome database (http://web.mit.edu/hyneslab/matrisome/) updated in August 2014, when the database comprised 1,110 genes coding for murine proteins in the ECM. Hierarchical clustering of the 113 proteins that were ascribed to the Mouse Matrisome was obtained using MeV software (v. 4.9.0) with $p < 0.01$ considered for statistical significance.

Immunohistochemistry, Immunofluorescence, and Confocal Analyses

Decellularized ECM samples were washed with PBS 1×, and whole-mount staining was performed. For DAPI staining, DAPI (Fluka-Sigma) was diluted in PBS 1× at 2 μg/mL and incubated for 5 min at room temperature. dECM was washed three times with PBS 1× and mounted with Mowiol (Calbiochem). For αLectin-PNA staining, dECM was washed with PBS 1× with 0.05% Tween (Sigma) (PBS-T) three times for 5 min and then incubated with αLectin-PNA (Alexa Fluor 594-conjugated peanut agglutinin lectin, L32459; Thermo Fisher) for 1 h at room temperature. dECM was then washed three times with PBS-T and mounted with Mowiol. For Sirius red collagen staining, dECMs were fixed with Bouin's solution (71% saturated picric acid solution, 8.5% formalin, and 4.8% glacial acetic acid) and then washed with tap water for 5 min. The sample was stained in Sirius red solution (0.1% Sirius red F3Ba dye in saturated picric acid solution) for 1 h at room temperature. The staining solution was discarded, samples were washed with 2% of acetic acid and then incubated with EtOH:picric acid (1:1) for 5 min. Finally, dECMs were dehydrated in EtOH, kept in a humid chamber until image acquisition and mounted with Mowiol. Microscopy images were obtained using a Nikon Eclipse TE200 fluorescence microscope, and final image processing was performed with ImageJ or Adobe Photoshop and Illustrator. For electron scanning microscopy, dECM was placed on a coverslip, dewaxed, dehydrated with absolute ethyl alcohol, and dried overnight in hexamethyldisilazane. Then, the sample was coated with gold-palladium after evaporation of hexamethyldisilazane and examined in a Leica S420 scanning electron microscope.

Generation of Pre-assembled Lympho-Organoids *In Vitro*

LOs were prepared by combining pSC and dECM. pSC cells (5×10^5) obtained from neonatal mLNs were resuspended in 500 μL of complete DMEM, seeded on top of dECM, and incubated at 37°C and 5% CO_2. After 2–3 h of incubation, cells were firmly adherent to dECM and could be packaged to obtain pre-LOs in 3D configuration and placed in ultra-low attachment 24-well plates (#3473, Corning). These 3D pre-assembled structures were incubated at 37°C and 5% CO_2 for 48 h for *in vitro* studies (immunofluorescence) and only overnight for *in vivo* experiments (transplantation).

Statistical Analyses

Data were analyzed using GraphPad Prism 5 (GraphPad Software). Statistical analysis was performed using a two-tailed unpaired Student's t test or χ^2 test, as indicated in the figure legends to evaluate statistical differences among the samples. An asterisk denotes statistical significance as follows: *$p < 0.05$, **$p < 0.01$, ***$p < 0.001$. All data are presented are as means ± SD. Group sizes were estimated based on pilot studies to determine the success rate and reproducibility of LO transplantation.

Data Availability

The authors declare that all data supporting the findings of this study are available within the manuscript or its supplementary files or are available from the corresponding author upon reasonable request.

AUTHOR CONTRIBUTIONS

E.L., S.B., S.T.P., L.G., M.T.P., L.R., A.S., and A.B. designed and performed experiments; M.A., T.V.P., S.M., and V.R. provided reagents and conceptual support; D.D. and A.A., generated and analyzed mass spectrometry data; E.L. and A.B. analyzed data, prepared figures, and wrote the manuscript; and A.B. directed the study.

(C) Scheme of LO transplantation and immunization. FACS plot of cells stained for Vα2 and Vβ5.1. LO, lympho-organoid; iLN, inguinal LN. Gating strategy for flow cytometry. FACS plot analysis of cells from inguinal LNs (iLNs) and LOs are shown. Quantification analysis of OT-I[+] CD8 T cells in LO and iLN. Data are presented as means ± SD from three different experiments. *p<0.05, **$p < 0.01$, and ***$p < 0.001$.

ACKNOWLEDGMENTS

REFERENCES

Alitalo, K. (2011). The lymphatic vasculature in disease. Nat. Med. *17*, 1371–1380.

Andersen, L., Hojris, I., Erlandsen, M., and Andersen, J. (2000). Treatment of breast-cancer-related lymphedema with or without manual lymphatic drainage–a randomized study. Acta Oncol. *39*, 399–405.

Becker, C., Assouad, J., Riquet, M., and Hidden, G. (2006). Postmastectomy lymphedema: long-term results following microsurgical lymph node transplantation. Ann. Surg. *243*, 313–315.

Benezech, C., Mader, E., Desanti, G., Khan, M., Nakamura, K., White, A., Ware, C.F., Anderson, G., and Caamano, J.H. (2012). Lymphotoxin-beta receptor signaling through NF-kappaB2-RelB pathway reprograms adipocyte precursors as lymph node stromal cells. Immunity *37*, 721–734.

Blum, K.S., Proulx, S.T., Luciani, P., Leroux, J.C., and Detmar, M. (2013). Dynamics of lymphatic regeneration and flow patterns after lymph node dissection. Breast Cancer Res. Treat. *139*, 81–86.

Brendolan, A., and Caamano, J.H. (2012). Mesenchymal cell differentiation during lymph node organogenesis. Front. Immunol. *3*, 381.

Castagnaro, L., Lenti, E., Maruzzelli, S., Spinardi, L., Migliori, E., Farinello, D., Sitia, G., Harrelson, Z., Evans, S.M., Guidotti, L.G., et al. (2013). Nkx2-5(+)islet1(+) mesenchymal precursors generate distinct spleen stromal cell subsets and participate in restoring stromal network integrity. Immunity *38*, 782–791.

Cupedo, T., Stroock, A., and Coles, M. (2012). Application of tissue engineering to the immune system: development of artificial lymph nodes. Front. Immunol. *3*, 343.

Farinello, D., Wozinska, M., Lenti, E., Genovese, L., Bianchessi, S., Migliori, E., Sacchetti, N., di Lillo, A., Bertilaccio, M.T.S., de Lalla, C., et al. (2018). A retinoic acid-dependent stroma-leukemia crosstalk promotes chronic lymphocytic leukemia progression. Nat. Commun. *9*, 1787.

Franco-Barraza, J., Beacham, D.A., Amatangelo, M.D., and Cukierman, E. (2016). Preparation of extracellular matrices produced by cultured and primary fibroblasts. Curr. Protoc. Cell Biol. *71*, 10.9.1–10.9.34.

Genovese, L., Zawada, L., Tosoni, A., Ferri, A., Zerbi, P., Allevi, R., Nebuloni, M., and Alfano, M. (2014). Cellular localization, invasion, and turnover are differently influenced by healthy and tumor-derived extracellular matrix. Tissue Eng. Part A *20*, 2005–2018.

Gould, D.J., Mehrara, B.J., Neligan, P., Cheng, M.H., and Patel, K.M. (2018). Lymph node transplantation for the treatment of lymphedema. J. Surg. Oncol. *118*, 736–742.

Hagerling, R., Pollmann, C., Kremer, L., Andresen, V., and Kiefer, F. (2011). Intravital two-photon microscopy of lymphatic vessel development and function using a transgenic Prox1 promoter-directed mOrange2 reporter mouse. Biochem. Soc. Trans. *39*, 1674–1681.

Kanapathy, M., Patel, N.M., Kalaskar, D.M., Mosahebi, A., Mehrara, B.J., and Seifalian, A.M. (2014). Tissue-engineered lymphatic graft for the treatment of lymphedema. J. Surg. Res. *192*, 544–554.

Kobayashi, Y., and Watanabe, T. (2016). Gel-trapped lymphorganogenic chemokines trigger artificial tertiary lymphoid organs and mount adaptive immune responses in vivo. Front. Immunol. *7*, 316.

Lim, J.F., Berger, H., and Su, I.H. (2016). Isolation and activation of murine lymphocytes. J. Vis. Exp. https://doi.org/10.3791/54596.

Lokmic, Z., Lammermann, T., Sixt, M., Cardell, S., Hallmann, R., and Sorokin, L. (2008). The extracellular matrix of the spleen as a potential organizer of immune cell compartments. Semin. Immunol. *20*, 4–13.

Naba, A., Clauser, K.R., Ding, H., Whittaker, C.A., Carr, S.A., and Hynes, R.O. (2016). The extracellular matrix: tools and insights for the "omics" era. Matrix Biol. *49*, 10–24.

Nosenko, M.A., Drutskaya, M.S., Moisenovich, M.M., and Nedospasov, S.A. (2016). Bioengineering of artificial lymphoid organs. Acta Naturae *8*, 10–23.

Onder, L., and Ludewig, B. (2018). A fresh view on lymph node organogenesis. Trends Immunol. *39*, 775–787.

Onder, L., Morbe, U., Pikor, N., Novkovic, M., Cheng, H.W., Hehlgans, T., Pfeffer, K., Becher, B., Waisman, A., Rulicke, T., et al. (2017). Lymphatic endothelial cells control initiation of lymph node organogenesis. Immunity *47*, 80–92.e84.

Petrova, T.V., and Koh, G.Y. (2018). Organ-specific lymphatic vasculature: from development to pathophysiology. J. Exp. Med. *215*, 35–49.

Proulx, S.T., Luciani, P., Christiansen, A., Karaman, S., Blum, K.S., Rinderknecht, M., Leroux, J.C., and Detmar, M. (2013). Use of a PEG-conjugated bright near-infrared dye for functional imaging of rerouting of tumor lymphatic drainage after sentinel lymph node metastasis. Biomaterials *34*, 5128–5137.

Proulx, S.T., Ma, Q., Andina, D., Leroux, J.C., and Detmar, M. (2017). Quantitative measurement of lymphatic function in mice by noninvasive near-infrared imaging of a peripheral vein. JCI Insight *2*, e90861.

Purwada, A., Jaiswal, M.K., Ahn, H., Nojima, T., Kitamura, D., Gaharwar, A.K., Cerchietti, L., and Singh, A. (2015). Ex vivo

engineered immune organoids for controlled germinal center reactions. Biomaterials *63*, 24–34.

Russo, V., Cipponi, A., Raccosta, L., Rainelli, C., Fontana, R., Maggioni, D., Lunghi, F., Mukenge, S., Ciceri, F., Bregni, M., et al. (2007). Lymphocytes genetically modified to express tumor antigens target DCs in vivo and induce antitumor immunity. J. Clin. Invest. *117*, 3087–3096.

Scaglioni, M.F., Arvanitakis, M., Chen, Y.C., Giovanoli, P., Chia-Shen Yang, J., and Chang, E.I. (2018). Comprehensive review of vascularized lymph node transfers for lymphedema: outcomes and complications. Microsurgery *38*, 222–229.

Suematsu, S., and Watanabe, T. (2004). Generation of a synthetic lymphoid tissue-like organoid in mice. Nat. Biotechnol. *22*, 1539–1545.